Electronic structure of a two-dimensional graphene monolayer in a spatially modulated magnetic field: Peierls tight-binding model

Y. H. Chiu,[1] Y. H. Lai,[2] J. H. Ho,[2] D. S. Chuu,[1,*] and M. F. Lin[2,†]
[1]*Institute of Physics, National Chiao Tung University, Hsinchu, Taiwan 300*
[2]*Department of Physics, National Cheng Kung University, Tainan, Taiwan 701*
(Received 3 May 2007; revised manuscript received 18 August 2007; published 11 January 2008)

Magnetoelectronic properties of a two-dimensional (2D) monolayer graphene are investigated by the Peierls tight-binding model. They are dominated by the period, strength, and direction of a spatially modulated magnetic field. Such a field could induce the reduction in dimensionality, change of energy dispersions, anisotropy at low energy, composite behavior in state degeneracy, extra band-edge states, and asymmetry of energy bands. There are partial flatbands at the Fermi level and one-dimensional parabolic bands at others. These make density of states exhibit delta-function-like structure and asymmetric prominent peaks, respectively. Energies of the extra band-edge states strongly depend on the period, while those of the original band-edge states exhibit little dependence. Both of them grow as the strength increases. The modulated and uniform magnetic fields differ from each other in energy dispersion, state degeneracy, and dimensionality. Important differences between a monolayer graphene and a 2D electron gas also exist.

DOI: 10.1103/PhysRevB.77.045407 PACS number(s): 73.20.At, 73.22.−f, 81.05.Uw

I. INTRODUCTION

Condensed-matter systems, such as diamond, layered graphenes, carbon nanotubes, carbon tori, C_{60}-related fullerenes, and carbon onions, are purely made up of carbon atoms. Such systems have very special symmetric configurations, and their dimensionalities vary from three dimensions to zero dimension. They could exhibit rich electronic properties, e.g., a wide-gap diamond, a semimetallic bulk graphite, a zero-gap monolayer graphene, a metallic armchair carbon nanotube, and a small-gap nonarmchair carbon nanotube. Recently, few-layer graphenes with two-dimensional (2D) hexagonal symmetry and nanoscaled thickness could be produced by controlling film thickness with single-atom accuracy.[1] Much research has been explored, such as growth,[2] phonon,[3] band structure,[4–7] electronic excitations,[8–11] optical spectra,[12,13] and transport properties.[14–20]

A 2D monolayer graphene owns linear bands intersecting at the Fermi level $E_F=0$. Energy bands are isotropic at low energy ($\lesssim$0.5 eV),[21] and so are the low-frequency physical properties (e.g., Coulomb excitations).[8,10] They produce a vanishing density of states at $E_F=0$, which makes a monolayer graphene an exotic zero-gap semiconductor. The two important characteristics, isotropy and semiconductor, originate from the hexagonal symmetric configuration. Electronic properties are completely changed by applying a uniform perpendicular magnetic field. Most of energy bands become the dispersionless Landau levels. The effective-mass model predicts that energies of the low Landau levels are proportional to the square root of field strength and quantum number.[22] These theoretical predictions have been verified by experimental measurements on transport properties[16] and optical spectra.[12] An inhomogeneous magnetic field might also strongly affect the essential physical properties. Haldane investigated whether a 2D graphene could exhibit magnetoconductance in the presence of a vanishing net magnetic field.[23] In this work, we focus mainly on the effects of a periodic magnetic field on electronic properties.

There have been numerous experimental[24–27] and theoretical[28–36] research for a two-dimensional electron gas (2DEG) under a spatially modulated magnetic field. These works primarily analyze the transport properties,[24–26,28,29] energy bands,[30–32] electronic excitations,[33–36] and optical spectra.[27] The transport measurements[24,25] manifest the oscillatory magnetoresistance. Energy bands of a 2DEG have parabolic energy dispersions. A periodic magnetic field leads to the drastic changes in electronic properties, e.g., the changes in state degeneracy, band-edge states, and curvatures.

The Peierls tight-binding model is used to calculate the electronic structure of a 2D graphene in a spatially modulated magnetic field. The Hamiltonian is a huge Hermitian matrix for a large modulation period ($\gtrsim$1000 Å). The numerical techniques are developed to attain a bandlike Hamiltonian matrix. The dependence of electronic properties on the direction, period, and strength of the modulated magnetic field will be investigated in detail, e.g., energy dispersions, state degeneracy, band-edge states, symmetry of energy bands, and density of states. A comparison with those of a uniform magnetic field is made. The important differences between a monolayer graphene and a 2DEG is also discussed.

This paper is organized as follows. The bandlike Hamiltonian matrix in a periodic magnetic field is derived in Sec. II. The main characteristics of the π-electronic structures are discussed in Sec. III. Finally, Sec. IV contains concluding remarks.

II. PEIERLS HAMILTONIAN BAND MATRIX

The tight-binding model with nearest-neighbor interactions is used to calculate the π-electronic structure of $2p_z$ orbitals. In the honeycomb structure of a 2D single-layer graphene in the absence of an external field, there are two kinds of carbon atoms, a and b, in a primitive unit cell. The wave function consisting of the two linear tight-binding

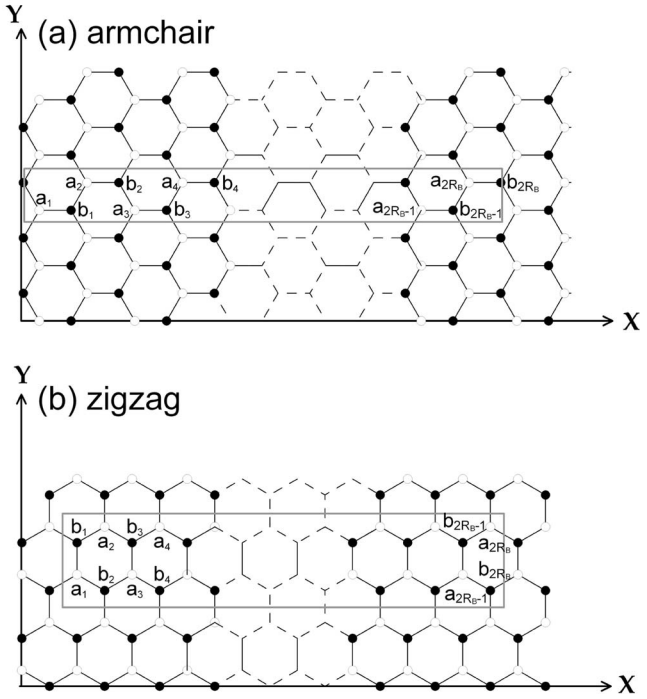

FIG. 1. The primitive unit cell of a monolayer graphene in the spatially modulated magnetic field with period R_B along (a) the armchair direction and (b) zigzag direction.

functions from periodic $2p_z$ orbitals is expressed as $|\Psi_{\mathbf{k}}\rangle = C_{a\mathbf{k}}|a_{\mathbf{k}}\rangle + C_{b\mathbf{k}}|b_{\mathbf{k}}\rangle$, where $|a_{\mathbf{k}}\rangle = \Sigma_i e^{i\mathbf{k}\cdot\mathbf{R}_i}|a_{i\mathbf{k}}\rangle$ and $|b_{\mathbf{k}}\rangle = \Sigma_j e^{i\mathbf{k}\cdot\mathbf{R}_j}|b_{j\mathbf{k}}\rangle$. The Hamiltonian built from $|a_{\mathbf{k}}\rangle$ and $|b_{\mathbf{k}}\rangle$ is a 2×2 Hermitian matrix. The site energies are vanishing ($\langle a_{i\mathbf{k}}|H_0|a_{i\mathbf{k}}\rangle = \langle b_{i\mathbf{k}}|H_0|b_{i\mathbf{k}}\rangle = 0$), and the nearest-neighbor hopping integral is given by

$$\langle b_{j\mathbf{k}}|H_0|a_{i\mathbf{k}}\rangle = \gamma_0 \exp[i\mathbf{k}\cdot(\mathbf{R}_i - \mathbf{R}_j)], \tag{1}$$

where γ_0(=2.56 eV) (Ref. 21) is the atom-atom interaction between two neighboring atoms at $\mathbf{R}_i$ and $\mathbf{R}_j$.

A monolayer graphene is assumed to exist in a spatially modulated magnetic field $\mathbf{B} = B\sin(Kx)\hat{z}$ along the armchair direction [the x axis in Fig. 1(a)], and the periodic length is $l_B = 2\pi/K = 3b'R_B$, where parameter R_B is useful in describing the dimensionality of the Hamiltonian matrix. The magnetic flux, product of the field strength and the hexagonal area in the unit of flux quantum ($\Phi_0 = hc/e = 4.1356 \times 10^{-15}$ T/m^2), is $\Phi = (3\sqrt{3}Bb'^2/2)/\Phi_0$. $b' = 1.42$ Å is the C–C bond length. The modulated magnetic field that leads to the Peierls phase is characterized by the vector potential $\mathbf{A} = -[B\cos(Kx)]/K\hat{y}$. The nearest-neighbor hopping integral becomes

$$\langle b_{j\mathbf{k}}|H_{\mathbf{B}}|a_{i\mathbf{k}}\rangle = \gamma_0 \exp\left\{ i\left[\mathbf{k}\cdot(\mathbf{R}_i - \mathbf{R}_j) + \frac{2\pi}{\Phi_0}\int_{\mathbf{R}_i}^{\mathbf{R}_j} \mathbf{A}\cdot d\mathbf{r} \right] \right\}. \tag{2}$$

For three nearest-neighbor atoms, their hopping integrals are, respectively, $t_{1\mathbf{k}}(n) = \gamma_0 \exp[(ik_x b'/2 + ik_y\sqrt{3}b'/2) + G_n]$, $t_{2\mathbf{k}}(n) = \gamma_0 \exp[(ik_x b'/2 - ik_y\sqrt{3}b'/2) - G_n]$, and $t_{3\mathbf{k}}(n) = \gamma_0 \exp(-ik_x b')$, where $G_n = -i[6(R_B)^2\Phi/\pi]\cos[\pi(n - 5/6)/R_B]\sin[(\pi/6R_B)]$. The modulation period causes the periodic boundary conditions along the x axis so that the corresponding Peierls phase is periodic in a period $2R_B$. An enlarged rectangular unit cell includes $4R_B$ carbon atoms. The wave function and the Hamiltonian matrix element are, respectively, given by

$$|\Psi_{\mathbf{k}}\rangle = \sum_{n=1}^{2R_B} C_{a\mathbf{k}}^n |a_{n\mathbf{k}}\rangle + C_{b\mathbf{k}}^n |b_{n\mathbf{k}}\rangle, \tag{3a}$$

$$\langle b_{m\mathbf{k}}|H_{\mathbf{B}}|a_{n\mathbf{k}}\rangle = [t_{1\mathbf{k}}(n) + t_{2\mathbf{k}}(n)]\delta_{m,n} + t_{3\mathbf{k}}(n)\delta_{m,n-1}. \tag{3b}$$

$C_{a\mathbf{k}}^n = C_{a\mathbf{k}}^{n+2R_B}$ and $C_{b\mathbf{k}}^n = C_{b\mathbf{k}}^{n+2R_B}$ are derived because of the periodical boundary condition. To solve the complicated calculations of the huge Hamiltonian matrix, the base functions are chosen as the following sequence

$$\{|a_{1\mathbf{k}}\rangle, |b_{2R_B\mathbf{k}}\rangle, |b_{1\mathbf{k}}\rangle, |a_{2R_B\mathbf{k}}\rangle, |a_{2\mathbf{k}}\rangle, |b_{2R_B-1\mathbf{k}}\rangle, |b_{2\mathbf{k}}\rangle, |a_{2R_B-1\mathbf{k}}\rangle, \ldots, |a_{R_B-1\mathbf{k}}\rangle, |b_{R_B+2\mathbf{k}}\rangle, |b_{R_B-1\mathbf{k}}\rangle, |a_{R_B+2\mathbf{k}}\rangle, |a_{R_B\mathbf{k}}\rangle, |b_{R_B+1\mathbf{k}}\rangle, |b_{R_B\mathbf{k}}\rangle; |a_{R_B+1\mathbf{k}}\rangle\}.$$

The Hamiltonian matrix could be expressed as a $4R_B \times 4R_B$ bandlike Hermitian matrix

$$\begin{pmatrix} 0 & q^* & p_1^* & 0 & \cdots & \cdots & 0 & 0 \\ q & 0 & 0 & p_{2R_B} & 0 & \cdots & \cdots & 0 \\ p_1 & 0 & 0 & 0 & q & 0 & \cdots & 0 \\ 0 & p_{2R_B}^* & 0 & 0 & 0 & q^* & 0 & 0 \\ \vdots & \ddots & q^* & 0 & 0 & \ddots & \ddots & 0 \\ \vdots & \cdots & \ddots & q & \ddots & \ddots & 0 & p_{R_B+1} \\ 0 & \vdots & \vdots & \ddots & \ddots & 0 & \ddots & q \\ 0 & 0 & 0 & 0 & 0 & p_{R_B+1}^* & q^* & 0 \end{pmatrix}, \tag{4}$$

where $p_n \equiv t_{1\mathbf{k}}(n) + t_{2\mathbf{k}}(n)$ and $q \equiv t_{3\mathbf{k}}$. Because the range of k_x is much smaller than that of k_y for a large R_B, it is sufficient just to consider one dimensional (1D) energy dispersions along k_y. That is to say, a modulated magnetic field could effectively reduce the dimensionality by 1.

The π-electronic structure strongly depends on the direction of the modulated magnetic field, mainly owing to the anisotropic structure of a 2D monolayer graphene. For the zigzag direction [Fig. 1(b)], the similar calculations could also be done. By the detailed derivations, the three hopping integrals are $t'_{1\mathbf{k}}(n) = \gamma_0 \exp[(ik_x\sqrt{3}b'/2 + ik_y b'/2) + G'_n]$, $t'_{2\mathbf{k}}(n) = \gamma_0 \exp[(-ik_x\sqrt{3}b'/2 + ik_y b'/2) - G'_{n-1}]$, and $t'_{3\mathbf{k}}(n) = \gamma_0 \exp[(-ik_y b') + G''_n]$, where $G'_n = -i[2(R_B)^2\Phi/3\pi]\cos[\pi(n - 1/2)/R_B]\sin(\pi/2R_B)$ and $G''_n = -i[(2R_B\Phi/3)\cos[(n - 1)\pi/R_B]]$. The Hamiltonian matrix element is further given by

$$\langle b_{m\mathbf{k}}|H_{\mathbf{B}}|a_{n\mathbf{k}}\rangle = t'_{1\mathbf{k}}(n)\delta_{m,n+1} + t'_{2\mathbf{k}}(n)\delta_{m,n-1} + t'_{3\mathbf{k}}(n)\delta_{m,n}. \tag{5}$$

With the base functions

$\{|a_{1\mathbf{k}}\rangle,|b_{2R_B\mathbf{k}}\rangle,|b_{1\mathbf{k}}\rangle,|a_{2R_B\mathbf{k}}\rangle,|b_{2\mathbf{k}}\rangle,|a_{2R_B-1\mathbf{k}}\rangle,|a_{2\mathbf{k}}\rangle,|b_{2R_B-1\mathbf{k}}\rangle,\ldots,|b_{R_B-1\mathbf{k}}\rangle,|a_{R_B+2\mathbf{k}}\rangle,|a_{R_B-1\mathbf{k}}\rangle,|b_{R_B+2\mathbf{k}}\rangle,|a_{R_B\mathbf{k}}\rangle,|b_{R_B+1\mathbf{k}}\rangle,|b_{R_B\mathbf{k}}\rangle;|a_{R_B+1\mathbf{k}}\rangle\}$,

the $4R_B\times 4R_B$ bandlike Hamiltonian matrix for the zigzag direction is

$$\begin{pmatrix}
0 & u_{2R_B}^* & v_1^* & 0 & s_1^* & 0 & \cdots & 0 & 0 & 0 \\
u_{2R_B} & 0 & 0 & v_{2R_B} & 0 & s_{2R_B-1} & 0 & 0 & 0 & 0 \\
v_1 & 0 & 0 & s_{2R_B} & \ddots & \ddots & \ddots & \ddots & 0 & 0 \\
0 & v_{2R_B}^* & s_{2R_B}^* & 0 & \ddots & & & \ddots & 0 & \vdots \\
s_1 & 0 & \ddots & \ddots & \ddots & & & \ddots & s_{R_B-1}^* & 0 \\
0 & s_{2R_B-1}^* & \ddots & & & \ddots & \ddots & \ddots & 0 & s_{R_B+1} \\
\vdots & 0 & \ddots & & & \ddots & 0 & s_{R_B}^* & v_{R_B}^* & 0 \\
0 & 0 & \ddots & \ddots & \ddots & \ddots & s_{R_B} & 0 & 0 & v_{R_B+1} \\
0 & 0 & 0 & 0 & s_{R_B-1} & 0 & v_{R_B} & 0 & 0 & u_{R_B} \\
0 & 0 & 0 & \cdots & 0 & s_{R_B+1}^* & 0 & v_{R_B+1}^* & u_{R_B}^* & 0
\end{pmatrix}, \tag{6}$$

where $s_n \equiv t'_{1\mathbf{k}}(n)$, $u_n \equiv t'_{2\mathbf{k}}(n)$, and $v_n \equiv t'_{3\mathbf{k}}(n)$. The Hamiltonian matrices in Eqs. (4) and (6), respectively, have two and three independent matrix elements.

III. MAGNETOELECTRONIC PROPERTIES

The unoccupied conduction bands (E^c's) are symmetric to the occupied valence bands (E^v's) about the Fermi level $E_F=0$. Only the former are discussed in this work. We first look at the low-energy bands resulting from the modulated magnetic field with period $R_B=1000$ along the armchair direction. At $B=0$, most of energy bands are parabolic dispersions with the double degeneracy except two nondegenerate linear bands intersecting at $E_F=0$ [the solid circles in Fig. 2(a)]. There is only one band-edge state in each energy band; furthermore, all the band-edge states are located at $k_y^{pp}=2\pi/3\sqrt{3}b'$ (the original band-edge states). The modulated magnetic field leads to drastic changes in band-edge states and energy dispersions, as shown in Fig. 2(a) by the open circles at $B=20$ T. The range of k_y, where electronic states could exist, becomes large. The linear bands are changed into partial flatbands at $E_F=0$. Also noted is that this result is similar to that of carbon nanotubes in magnetic fields perpendicular to the symmetry axis.[37] The doubly degenerate parabolic bands have weak energy dispersions or low curvatures at k_y^{pp}, and their number is largely reduced. Such effects suggest that a magnetic field could make electronic states flock together. The modulation effects of **B** on parabolic energy bands result in four extra band-edge states at k_y^{sp}'s, the strong energy dispersions close to k_y^{sp}'s, and the destruction of the double degeneracy. The two extra band-edge states at the left- and right-hand sites of k_y^{pp} might have different energies; that is, one side of the parabolic bands might be asymmetric to the other about the original band-edge states. Each parabolic band exhibits the composite behavior in state degeneracy, the single and double degeneracies near k_y^{sp} and k_y^{pp}, respectively.

The number of subbands grows quickly as state energy E^c increases from zero. There are many middle energy bands

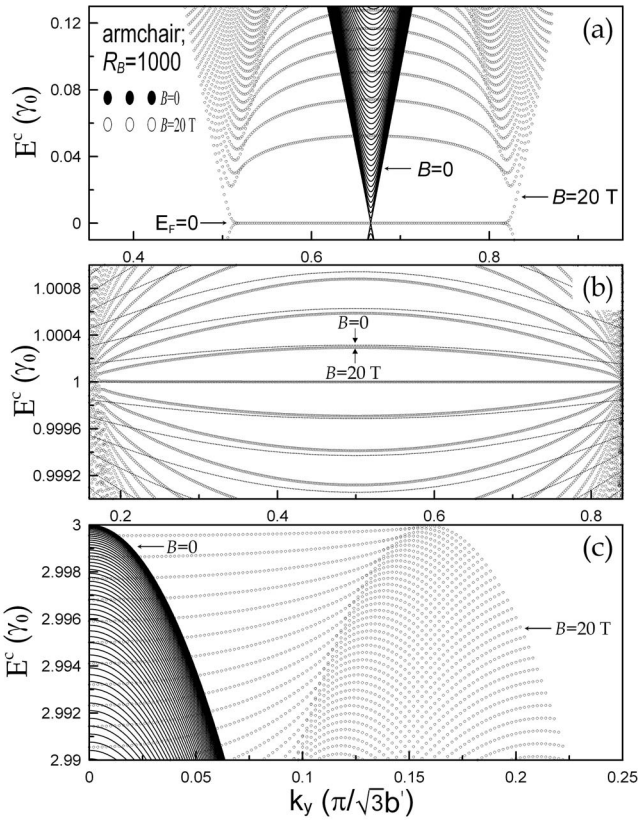

FIG. 2. Energy bands near (a) $E^c=0$, (b) $E^c=\gamma_0$, and (c) $E^c=3\gamma_0$ for the armchair modulation direction at $R_B=1000$ and $B=20$ T. Those without B are also shown for comparison.

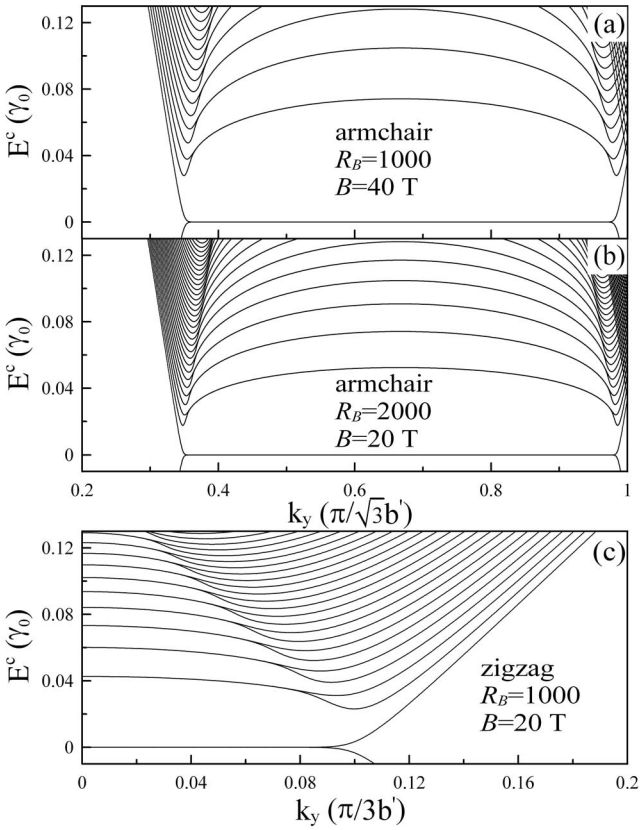

FIG. 3. The low-energy bands along the armchair direction at (a) R_B=1000, B=40 T and (b) R_B=2000, B=20 T, and those along (c) the zigzag direction at R_B=1000, B=20 T.

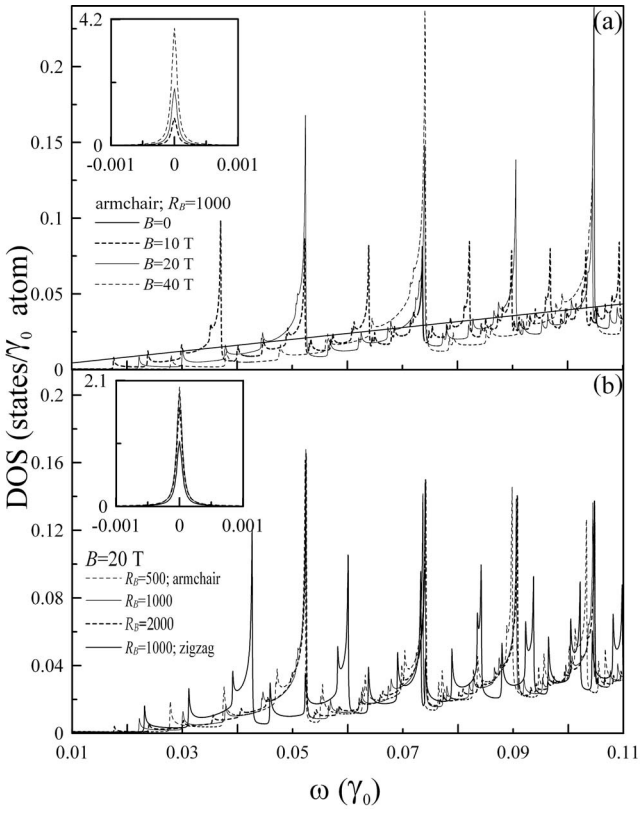

FIG. 4. The low-frequency density of states (a) along the armchair direction at R_B=1000 and different B's and (b) at B=20 T and different R_B's or directions. The insets show those near E_F=0.

near $E^c \simeq \gamma_0$, as shown in Fig. 2(b). At B=0, they include complete flatbands at $E^c=\gamma_0$ and parabolic bands at the others. Both are doubly degenerate. The parabolic bands have a low curvature at $k_y^{pp}=\pi/2\sqrt{3}b'$ and a high curvature at k_y^{sp} =0 (not shown). Moreover, in the small or large k_y, the modulated magnetic field could destroy double degeneracy and create extra band-edge states. It modifies the band curvatures at k_y^{pp}, and makes the complete flatbands change into the partial flatbands.

The subband number decreases gradually with the further increase of state energy. The high-energy bands, as shown in Fig. 2(c) for B=0, are parabolic dispersions with the double degeneracy and one band-edge state at k_y^{pp}=0. All the k_y^{pp} states remain unchanged in the presence of **B**, as seen in low and middle energy bands. However, the modulated magnetic field could reduce the number of subbands or widen the range of k_y, produce the extra band-edge states at $k_y^{sp} \neq 0$, and induce the composite behavior of the single and double degeneracies.

The strength, period, and direction of the modulated magnetic field strongly affect the electronic structure, as shown in Figs. 3(a) and 3(b) for the low-energy bands. The range of partial flatbands increases with increasing B, while their number and curvatures exhibit the opposite behavior [Figs. 3(a) and 2(a)]. These results further demonstrate that the ability to flock electronic states is enhanced by the increasing field strength. The longer the period, the larger the effective range of k_y [Figs. 3(b) and 2(a)]. The period could alter state energies and curvatures of extra band-edge states at k_y^{sp}'s. It is also worth noting that $k_y^{pp}=2\pi/3\sqrt{3}b'$ of the doubly degenerate parabolic bands is independent of period and strength. When the spatially modulated direction is along the zigzag structure, there are two partial flatbands at E_F=0 and many parabolic bands at the others [Fig. 3(c)]. The former are doubly degenerate; the latter are fourfold degenerate near k_y^{pp}=0 and doubly degenerate near k_y^{sp}. That state degeneracy, subband number, k_y's of band-edge states, and range of partial flatbands depend on the modulation direction, which directly reflects the anisotropic characteristic of a graphene geometry. In addition, the similar effects could also be found in moderate and high-energy bands.

Density of states (DOS), which is closely related to essential features of the electronic structure, is defined as

$$D(\omega) = \sum_{\sigma,h=c,\nu} \int_{1\text{stBZ}} \frac{dk_x dk_y}{(2\pi)^2} \frac{\Gamma}{\pi} \frac{1}{[E^h(k_x,k_y)-\omega]^2+\Gamma^2}. \quad (7)$$

$\Gamma(=10^{-4}\gamma_0)$ is a phenomenological broadening parameter. The integration on k_x could be roughly neglected because of the very small range of k_x. The low-frequency DOS at B=0 is proportional to ω, as shown in Fig. 4(a). It vanishes at ω =0 and has no special structures. However, the modulated magnetic field leads to a symmetric delta-function-like peak at ω=0 [inset in Fig. 4(a)] and considerable asymmetric square-root divergent peaks. The former comes from the two partial flatbands at E_F=0, and its height grows with the in-

creasing field strength. The latter are dominated by the band-edge states of the 1D parabolic dispersions along $\hat{k}_y$ [Fig. 2(a)]. The asymmetric pronounced peaks could be further divided into weak subpeaks and strong principal peaks. They are, respectively, due to the band-edge states at k_y^{sp}'s and k_y^{pp}. There are many pairs of subpeaks, and each pair of subpeaks is associated with the asymmetry of the 1D parabolic bands about the k_y^{pp} states [discussed earlier in Fig. 2(a)]. The number, frequencies, and heights of the asymmetric prominent peaks are sensitive to the changes in the strength, period, and modulation direction. The peak number decreases with the increase of the strength, while the peak frequencies exhibit a different behavior [Fig. 4(a)]. The number of subpeaks increases as the period grows [Fig. 4(b)], while it is the other way around as the frequencies of subpeaks increase. The main features of principal peaks have the weak dependence on the period. When the modulation direction is orientated relatively close to the zigzag structure, more principal peaks with lower frequencies are observed [comparison between the heavy and light solid curves in Fig. 4(b)]. Density of states could display the high anisotropy even at very low frequency [$\omega \to 0$ in the inset of Fig. 4(b)]. However, the low-frequency physical properties without **B** are anisotropic only for $\omega \gtrsim 0.25\gamma_0$, e.g., electronic excitations and absorption spectra.[9] This result indicates that the anisotropy of the low-frequency electronic properties could be induced by means of a spatially modulated magnetic field.

The frequencies of prominent peaks in DOS deserve a closer investigation. Figure 5(a) shows the relation between the frequencies (ω_{sp}'s) of the first six subpeaks and the period at $B=20$ T. These peaks correspond to the extra band-edge states at the left-hand neighborhood of k_y^{pp} [Fig. 2(a)]. ω_{sp}'s decline quickly as R_B increases. As to the frequencies of principal peaks (ω_{pp}'s), their dependence on the period is minor for a sufficient large R_B ($\gtrsim 1000$), as shown in Fig. 5(b). Both ω_{sp}'s and ω_{pp}'s are largely enhanced by the increasing field strength [Figs. 5(c) and 5(d)]. There exists a special square-root relation between ω_{pp} and B, i.e., $\omega_{pp} \propto \sqrt{B}$. In addition, the low-energy flat Landau levels due to a uniform magnetic field ($\mathbf{B}_0$) also exhibit the square-root dependence on the field strength.[22] The band-edge state energies are closely related to the magneto-optical absorption frequencies. The predicted results could be verified by the optical spectroscopy.

A uniform magnetic field differs from a spatially modulated magnetic field in the low-energy magnetoelectronic structures. In terms of the ability in flocking electronic states, the former is much stronger than the latter. A uniform magnetic field could make linear or parabolic bands convert into the dispersionless Landau levels. Such levels are fourfold degenerate for each k_y state. All the Landau states could be regarded as the band-edge states. They would exhibit zero-dimensional features, but not one-dimensional features. For example, the magneto-optical absorption spectra display the symmetric and asymmetric prominent peaks in cases $\mathbf{B}_0$ and **B**, respectively.

The electronic structure of a 2DEG could be strongly affected by a spatially modulated magnetic field.[30–32] It also displays the similar behaviors to a monolayer graphene, such

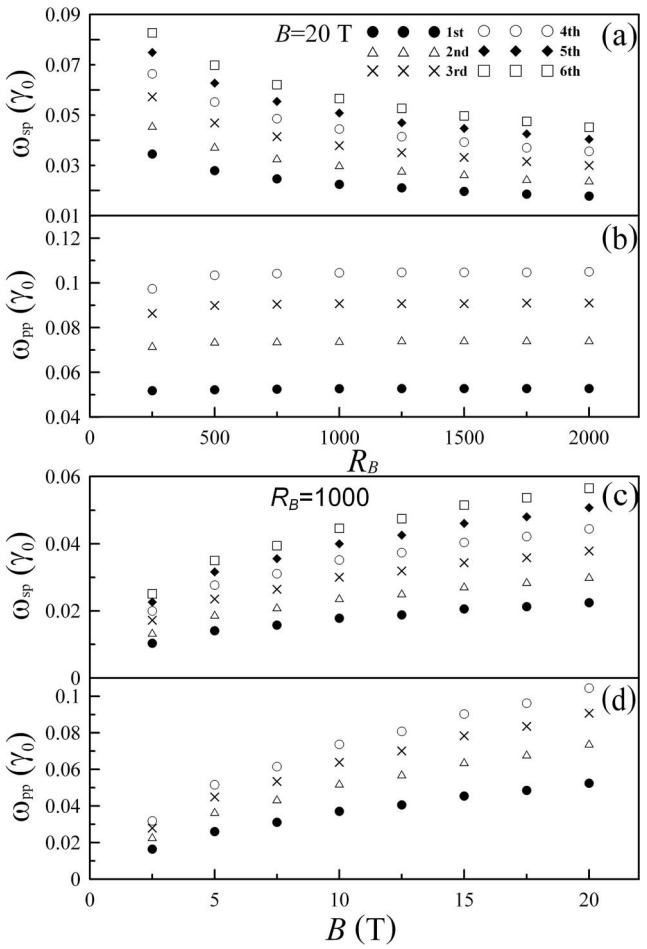

FIG. 5. Energies (ω_{sp}'s) of extra band-edge states at the left-hand neighborhood of k_y^{pp} and those (ω_{pp}'s) of the original band-edge states. (a) and (b) are their dependences on the period; (c) and (d) correspond to the dependence on the strength.

as the composite behavior in state degeneracy, creation of extra band-edge states, and change of curvatures. However, there are three significant differences between a 2DEG and a monolayer graphene. A 2DEG does not exhibit partial flat-bands at zero energy. Its magnetoelectronic structure is independent of the modulation direction. Moreover, the wave vectors of extra band-edge states are approximately close to $k_y=0$ and hardly depend on the state energy. The above-mentioned differences mainly come from the hexagonal structure of a monolayer graphene.

IV. CONDLUDING REMARKS

In summary, the magnetoelectronic structure of a 2D monolayer graphene is studied by the Peierls tight-binding model. The specific base functions are chosen to solve a huge Hamiltonian matrix. The strength, period, and direction of a spatially modulated magnetic field dominate the main features of electronic properties. Such a field could reduce dimensionality by 1, alter energy dispersions, cause anisotropy at low energy, induce composite behavior in state degeneracy (the composite behavior of single and double de-

generacies for the armchair direction), produce extra band-edge states, and destroy the symmetry of energy bands about the original band-edge states. Energies of the extra band-edge states strongly rely on the period, while the opposite is true for those of the original band-edge states. Both of them grow with the increase of the strength. Density of states owns many asymmetric prominent peaks, mainly owing to the band-edge states in 1D parabolic bands. The partial flatbands also make DOS display delta-function-like structures at the Fermi level. A spatially modulated magnetic field contrasts sharply with a uniform magnetic field in energy dispersion, state degeneracy, and dimensionality. The important differences between a monolayer graphene and a 2DEG arise from the hexagonal symmetry. They are the existence of the partial flatbands at zero energy, dependence on the modulation direction, and wave vectors of the band-edge states. The experimental measurements on the magneto-optical absorption spectra could be utilized to examine the predicted electronic properties.

ACKNOWLEDGMENTS

This work was supported by NSC and NCTS of Taiwan, under the Grant Nos. NSC 95-2112-M-006-028-MY3 and NSC 95-2119-M-009-030.

*dschuu@mail.nctu.edu.tw
†mflin@mail.ncku.edu.tw

[1] K. S. Novoselov, A. K. Geim, S. V. Morozov, D. Jiang, Y. Zhang, S. V. Dubonos, I. V. Grigorieva, and A. A. Firsov, Science **306**, 666 (2004).
[2] C. Berger, Z. Song, T. Li, X. Li, A. Y. Ogbazghi, R. Feng, Z. Dai, A. N. Marchenkov, E. H. Conrad, P. N. First, and W. A. de Heer, J. Phys. Chem. B **108**, 19912 (2004).
[3] A. H. Castro Neto and F. Guinea, Phys. Rev. B **75**, 045404 (2007).
[4] C. P. Chang, C. L. Lu, F. L. Shyu, R. B. Chen, Y. K. Fang, and M. F. Lin, Carbon **42**, 2975 (2004).
[5] F. Guinea, A. H. Castro Neto, and N. M. R. Peres, Phys. Rev. B **73**, 245426 (2006).
[6] S. Latil and L. Henrard, Phys. Rev. Lett. **97**, 036803 (2006).
[7] E. McCann, Phys. Rev. B **74**, 161403(R) (2006).
[8] F. L. Shyu and M. F. Lin, J. Phys. Soc. Jpn. **69**, 607 (2000).
[9] J. H. Ho, C. P. Chang, and M. F. Lin, Phys. Lett. A **352**, 446 (2006).
[10] J. H. Ho, C. L. Lu, C. C. Hwang, C. P. Chang, and M. F. Lin, Phys. Rev. B **74**, 085406 (2006).
[11] X. F. Wang and T. Chakraborty, Phys. Rev. B **75**, 041404(R) (2007).
[12] M. L. Sadowski, G. Martinez, M. Potemski, C. Berger, and W. A. de Heer, Phys. Rev. Lett. **97**, 266405 (2006).
[13] L. Joly, L. Tati-Bismaths, and W. Weber, Phys. Rev. Lett. **97**, 187404 (2006).
[14] J. S. Bunch, Y. Yaish, M. Brink, K. Bolotin, and P. L. McEuen, Nano Lett. **5**, 287 (2005).
[15] K. S. Novoselov, E. McCann, S. V. Morozov, V. I. Fal'ko, M. I. Katsnelson, U. Zeitler, D. Jiang, F. Schedin, and A. K. Geim, Nat. Phys. **2**, 177 (2006).
[16] K. S. Novoselov, A. K. Geim, S. V. Morozov, D. Jiang, M. I. Katsnelson, I. V. Grigorieva, S. V. Dubonos, and A. A. Firsov, Nature (London) **438**, 197 (2005).
[17] Y. Zhang, Y. W. Tan, H. L. Stormer, and P. Kim, Nature (London) **438**, 201 (2005).
[18] K. S. Novoselov, Z. Jiang, Y. Zhang, S. V. Morozov, H. L. Stormer, U. Zeitler, J. C. Maan, G. S. Boebinger, P. Kim, and A. K. Geim, Science **315**, 1379 (2007).
[19] V. P. Gusynin and S. G. Sharapov, Phys. Rev. Lett. **95**, 146801 (2005).
[20] E. McCann and V. I. Fal'ko, Phys. Rev. Lett. **96**, 086805 (2006).
[21] P. R. Wallace, Phys. Rev. **71**, 622 (1947).
[22] J. W. McClure, Phys. Rev. **104**, 666 (1956).
[23] F. D. M. Haldane, Phys. Rev. Lett. **61**, 2015 (1988).
[24] H. A. Carmona, A. K. Geim, A. Nogaret, P. C. Main, T. J. Foster, M. Henini, S. P. Beaumont, and M. G. Blamire, Phys. Rev. Lett. **74**, 3009 (1995).
[25] P. D. Ye, D. Weiss, R. R. Gerhardts, M. Seeger, K. von Klitzing, K. Eberl, and H. Nickel, Phys. Rev. Lett. **74**, 3013 (1995).
[26] Mayumi Kato, Akira Endo, Makoto Sakairi, Shingo Katsumoto, and Yasuhiro Iye, J. Phys. Soc. Jpn. **68**, 1492 (1999).
[27] S. Cina, D. M. Whittaker, D. D. Arnone, T. Burke, H. P. Hughes, M. Leadbeater, M. Pepper, and D. A. Ritchie, Phys. Rev. Lett. **83**, 4425 (1999).
[28] P. Vasilopoulos and F. M. Peeters, Superlattices Microstruct. **7**, 393 (1990).
[29] F. M. Peeters and P. Vasilopoulos, Phys. Rev. B **47**, 1466 (1993).
[30] I. S. Ibrahim and F. M. Peeters, Phys. Rev. B **52**, 17321 (1995).
[31] Andrey Krakovsky, Phys. Rev. B **53**, 8469 (1996).
[32] A. Y. Rom, Phys. Rev. B **55**, 11025 (1997).
[33] J. M. Luttinger, Phys. Rev. **84**, 814 (1951).
[34] S. M. Stewart and C. Zhang, Semicond. Sci. Technol. **10**, 1541 (1995).
[35] S. M. Stewart and C. Zhang, Phys. Rev. B **52**, R17036 (1995).
[36] S. M. Stewart and C. Zhang, J. Phys.: Condens. Matter **8**, 6019 (1996).
[37] H. Ajiki and T. Ando, J. Phys. Soc. Jpn. **64**, 260 (1995).